Molecular Therapy
Nucleic Acids
Original Article

Aminoglycoside Enhances the Delivery of Antisense Morpholino Oligonucleotides *In Vitro* and in *mdx* Mice

Mingxing Wang,[1] Bo Wu,[1] Sapana N. Shah,[1] Peijuan Lu,[1] and Qilong Lu[1]

[1]McColl-Lockwood Laboratory for Muscular Dystrophy Research, Department of Neurology, Cannon Research Center, Carolinas Medical Center, 1000 Blythe Blvd., Charlotte, NC 28203, USA

Antisense oligonucleotide (AO) therapy has been the specific treatment for Duchenne muscular dystrophy, with ongoing clinical trials. However, therapeutic applications of AOs remain limited, particularly because of the lack of efficient cellular delivery methods imperative for achieving efficacy. In this study, we investigated a few aminoglycosides (AGs) for their potential to improve the delivery of antisense phosphorodiamidate morpholino oligomer (PMO) both *in vitro* and *in vivo*. AGs had lower cytotoxicity compared with Endoporter, the currently most effective delivery reagent for PMO *in vitro*, and improved efficiency in PMO delivery 9- to 15-fold over PMO alone. Significant enhancement in systemic PMO-targeted dystrophin exon 23 skipping was observed in *mdx* mice, up to a 6-fold increase with AG3 (kanamycin) and AG7 (sisomicin) compared with PMO only. No muscle damage could be detected clearly with the test dosages. These results establish AGs as PMO delivery-enhancing agents for treating muscular dystrophy or other diseases.

INTRODUCTION

Duchenne muscular dystrophy (DMD), characterized by progressive muscle degeneration, is an X-linked inherited muscle disorder caused by nonsense or frameshift mutations in the dystrophin gene, affecting approximately 1 in 5,000 live male births.[1–4] Fundamental treatments of DMD require either correction of the mutated gene or supplementing a normal copy of the gene to restore function. The large size of dystrophin protein and the requirement of lifetime administration to muscles throughout the body severely limit progress in developing effective experimental therapies.[5] Antisense oligonucleotide (AO)-mediated exon skipping has been demonstrated recently to be promising for treatment of DMD by intentionally skipping one or multiple exons to restore the normal reading frame of the mutated transcripts, resulting in production of internally truncated but functional dystrophin proteins.[6–15] AOs are short, single-stranded sequences of synthetic and chemically modified RNA or DNA capable to hybridize to specific targets by Watson-Crick base-pairing rules. They are easier to scale up for Good Manufacturing Practice (GMP) production than viral vectors or therapeutic cells.[16] Of the synthetic oligonucleotides, phosphorodiamidate morpholino oligomer (PMO) is the most commonly studied AO for exon skipping in the dystrophin gene and has been approved by the US Food and Drug Administration (FDA) as the only oligonucleotide drug specific to DMD.[6,7,10,17,18] PMOs have phosphorodiamidate linkages and morpholino rings instead of deoxyribose rings, being neutral under physiological condition. These modifications confer nuclease resistance and enhanced binding to mRNA, and prevent RNaseH activity, and lower toxicity compared with other counterparts.[19,20] However, the uncharged nature of PMOs is associated with poor cell uptake and fast clearance in the bloodstream, which dramatically impedes pharmacological outcomes. Studies in several animal models have demonstrated that a significant therapeutic effect on DMD can be achieved as follows. (1) Increasing doses of PMOs could be used, but this could be cost-prohibitive and have an increased risk of toxicity, especially for long-term systemic administration.[13] (2) Chemical modification with cell-penetrating peptide-POMO conjugate (PPMO) or guanidine-rich dendrimer (Vivo-PMO) has been reported to have a significantly heightened effect, leading to nearly normal levels of dystrophin expression in muscles throughout the whole-body by systemic delivery.[11–15] However, the packed cationic charges are associated with higher toxicity, posing considerable risk for long-term clinical applications.[11,14] Potential peptide-related immune responses might also prevent repeated administration. Furthermore, the complicated synthesis and purification procedures increase the cost. (3) An amphiphilic polymer-mediated delivery strategy has been studied recently by us and has been demonstrated to be promising *in vitro* and in *mdx* mice *in vivo*.[21–24] (4) Small-molecule-aided approaches could be used, including the dantrolene for PMO delivery,[25] monosaccharide-formulated AOs,[26,27] and saponin-mediated PMO delivery.[28] Although promising results have been demonstrated by the aforementioned approaches, efficient and safe delivery of PMO to achieve long-term significant therapeutic results for the treatment of DMD remains a huge challenge.

Aminoglycosides (AGs) are composed of amino sugar and aminocyclitol by oxygen bridge connection. It is a group of highly potent

Received 28 January 2019; accepted 23 April 2019;
https://doi.org/10.1016/j.omtn.2019.04.023.

Correspondence: Mingxing Wang, McColl-Lockwood Laboratory for Muscular Dystrophy Research, Department of Neurology, Cannon Research Center, Carolinas Medical Center, 1000 Blythe Blvd., Charlotte, NC 28203, USA
E-mail: mingxing.wang@atriumhealth.org

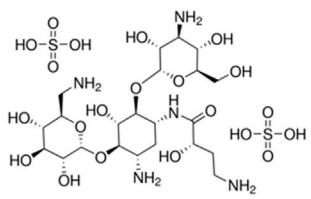

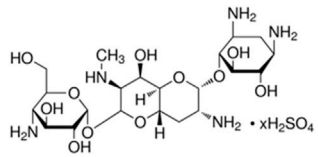

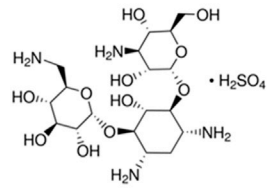

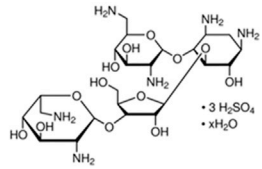

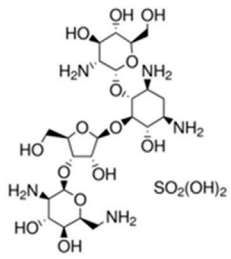

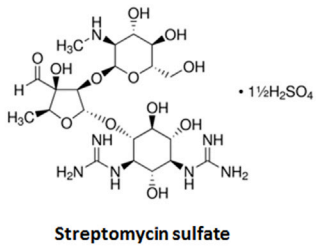

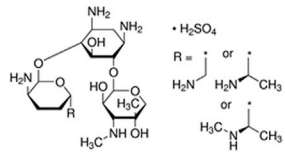

Code	Name
AG1	Amikacin
AG2	Apramycin sulfate
AG3	Kanamycin A sulfate
AG4	Neomycin sulfate
AG5	Paromomycin sulfate
AG6	Streptomycin sulfate
AG7	Sisomicin sulfate
AG8	Gentamicin sulfate

Figure 1. Chemical Structures, Names, and Code Numbers of AGs

antibiotics in use for almost six decades because of their enormous therapeutic value.[29,30] For example, gentamicin and amikacin are used to treat meningitis, pneumonia, and sepsis;[31–33] paromomycin is used for amebic dysentery;[34] neomycin is used for ulcers and dermatitis;[35] and gentamicin has also been reported to restore dystrophin function expression to the skeletal muscles of *mdx* mice by readthrough.[36–39] AGs have binding capabilities with many different functional RNAs and have become a central focus in an effort to understand the underlying principles of RNA recognition by small molecules.[40–47] In view of AG structure characteristics and binding capabilities with different functional RNAs, we surmised that AGs might be used as a nonionic, biocompatible, biodegradable delivery vector for the AO PMO by forming a stable complex for the treatment of muscular dystrophy. We chose to investigate a few AGs that are commercially available and have been widely used as biomaterials. Here we describe the results of using AGs for the delivery of PMO in cell culture and *in vivo* in *mdx* mice.

RESULTS AND DISCUSSION

The AGs investigated in this study are all available commercially available, and their structures, brand names, and code numbers are shown in Figure 1.

Cytotoxicity

Cytotoxicity of the AGs was determined using an MTS (3-(4,5-dimethylthiazol-2-yl)-5-(3-carboxymethoxyphenyl)-2-(4-sulfophenyl)-2H-tetrazolium)-based assay in C2C12E50 myoblast cells using a range of AG concentrations (from 5 μg/mL to 100 μg/mL), as shown in Figure 2. Cytotoxicity was determined in relation to the numbers of amino groups and the basicity of a given amino group in a given AG: the more amino groups or the more basic of a given amino group in an AG molecule, the more toxic it is. For instance, AG8 and AG6 having more basic-amino groups, AG4 owning more amino groups than others, they showed more toxicity compared with other counterparts at higher doses. This correlated well with what has been reported previously Hainrichson et al.[48] All selected AGs had much lower cytotoxicity compared with Endoporter, arguably the most effective and commercially available vector for PMO delivery *in vitro*. The proportion of live cells remained over 70% with almost all AGs, except for AG8 (65%), but less than 20% with Endoporter at the highest dose of 100 μg/mL.

Delivery of PMO with AGs *In Vitro*

C2C12E50 myoblasts stably expressing a GFP reporter bifurcated by insertion of human dystrophin exon 50 (hDysE50) was used to evaluate the efficacy of AGs for the delivery of PMO.[49,50] The expression of GFP in the reporter cells relies on the targeted skip of exon 50 by AOs. A PMO sequence, PMOE50 (5′-AACTTCCTCTTTAACA GAAAAGCATAC-3′), with previously confirmed efficacy for targeted removal of hDysE50 was used.[49] The reporter cells were treated with a fixed amount (5 μg) of PMOE50 in 500 μL 10% fetal bovine serum (FBS)-DMEM formulated with each of the AGs at escalating doses of 10, 20, and 50 μg. Transfection efficiency, represented by the levels of GFP expression, was determined by fluorescence-activated cell sorting (FACS) analysis (Figure 3). The results showed that AGs at 10 μg significantly improved PMOE50-induced GFP expression compared with PMOE50 alone, and the transduction efficiency, as GFP-positive cells, was up to 50%–63% at higher doses for AG3, AG5, AG6, and AG7, 12- to 15-fold higher than PMO only, which produced approximately 4% efficiency. The degrees of efficacy with AGs were lower than that (>80%) achieved with Endoporter at its optimal dosage recommended by the manufacturer. The levels of GFP expression were also structure-dependent. AG, the smaller amino sugar with a less positive charge,

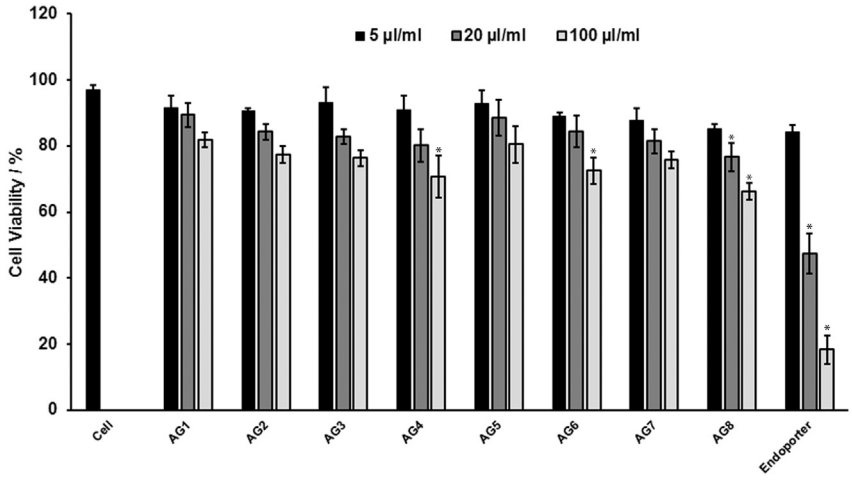

Figure 2. Viability of C2C12E50 Myoblasts after Treatment with AGs at 3 Doses (5, 20, and 100 μg/mL; Endoporter as a Control), Determined by MTS Assay

Cells were seeded in 96-well plate at an initial density of 1×10^4 cells/well in 0.2 mL growth medium. The results are presented as the mean ± SD in triplicate (one-way ANOVA, no significant difference between AG groups; Student's t test, *$p \leq 0.05$ compared with untreated cells).

demonstrated moderate transduction efficiency for PMO delivery compared with Endoporter, a rich, positively charged amphiphilic peptide explicitly designed to deliver PMO into the cytosol of cells by an endocytosis-mediated process. The larger the molecules and/or the more hydrophobic they are, the more effective they are as PMO delivery vectors *in vitro*, which has been confirmed in our previous study.[20–23] Nevertheless, differences in efficacy with all AGs were limited for PMO delivery, probably because of their similarity in molecular size and the number of amino groups. However, guanidinylation of AG6 had a somewhat better performance than other AGs. This is in agreement with a previous report showing that AGs generally exhibit poor uptake by eukaryotic cell lines but that guanidinylation of the AGs dramatically enhances cellular uptake.[51,52] The exon-skipping efficiency was clearly dose-dependent, and cytotoxicity remained similar to that of AGs used alone, with live cells being over 75% at the highest dosage.

We also examined the potential of the AGs for PMO delivery in myotubes, which are more relevant to muscle fibers *in vivo*.[53] C2C12 cells stably express the GFP protein disrupted by mouse bifurcated dystrophin exon 23 (C2C12E23). Expression of the reporter construct was driven by a muscle creatine kinase (MCK) promoter, allowing us to evaluate the exon skipping of AOs in differentiating cells and differentiated myotubes. For this purpose, cell cultures reaching around 70% confluence were incubated in differentiation medium for 2 days when myotubes were clearly abundant. The cell cultures were then treated with PMOE23 (5 μg) formulated with AGs at three dosages (10, 20, and 50 μg in 0.5 mL medium, based on the results from PMOE50 delivery), and Endoporter (5 μg) was used as a control. Fluorescence images showed a similar trend in efficiency as that achieved in C2C12E50 cells for PMOE50 delivery by the individual AGs, as illustrated in Figure 4. The results demonstrated that AGs can improve the delivery efficiency of PMO in both myoblasts and myotubes. The enhanced delivery of PMO formulated with AGs can probably be attributed to the stable complex and prolonged circulation that result from hydrogen binding between AGs and PMO oligonucleotides and the inherent conformational adaptability of AG to oligonucleotides.[54,55]

Delivery of PMO with AGs *In Vivo*

Local Delivery

We next evaluated the effect of AGs for PMO delivery *in vivo* by intramuscular (i.m.) injection in *mdx* mice. These mice contain a nonsense mutation in exon 23, preventing production of functional dystrophin protein. PMOE23 targeting dystrophin exon 23 was injected into the *tibialis anterior* (TA) muscle, and removal of the mutated exon 23 restored the reading frame of dystrophin transcripts, which can be seen by expression of a truncated dystrophin protein. Based on the delivery performance *in vitro*, we chose 50 μg AGs premixed with 2 μg of PMOE23 in 40 μL saline for injection. The same amount of PMOE23 only was used as a control. The treated TA muscles were harvested 2 week later.

Immunohistochemistry showed that mice treated with AG-formulated PMOE23 had dramatically increased numbers of dystrophin-positive fibers, up to 42%, 55%, 45%, and 62% in one cross-section of the TA muscle for AG1-, AG3-, AG5-, and AG7-formulated PMOs, respectively, and reaching 5- or 6-fold with AG3 and AG7 compared with the control PMO, which produced only 10% positive fibers. The levels of exon skipping and corresponding dystrophin expression were also determined by RT-PCR and western blot. AG-formulated PMO achieved levels of exon-skipping of 45.1% (AG1), 32.7% (AG2), 39.3% (AG3), 34.2% (AG4), 36.3% (AG5), 33.4% (AG6), 47.8% (AG7), and 37.9% (AG8) compared with 22.4% for PMO alone and dystrophin protein expression in the following order: AG7, AG5 > AG1, AG3, AG4 > AG2, AG6, AG8-formulated PMO > PMO alone (C57 normalized as 100%) (Figure 5). These results correlated well with the data in muscle cell lines *in vitro*. Interestingly, AG8 (gentamicin) did not have higher efficiency than the other AGs, despite the reported ability to restore dystrophin expression in skeletal muscles of *mdx* mice by suppressing nonsense mutations.[10] Taken together, these results demonstrate the following. (1) AGs are potent to improve the delivery efficiency of PMO oligonucleotide. This effect is likely related to the probable formation of hydrogen binding between AGs and PMO oligonucleotides and the inherent conformational adaptability of AG to oligonucleotide PMOs, which consequently condense and stabilize the AG/PMO complex, leading to improved delivery efficiency. (2) The positive charge from the amino group of AGs provides benefits to the uncharged PMO for interaction with the cell membrane and

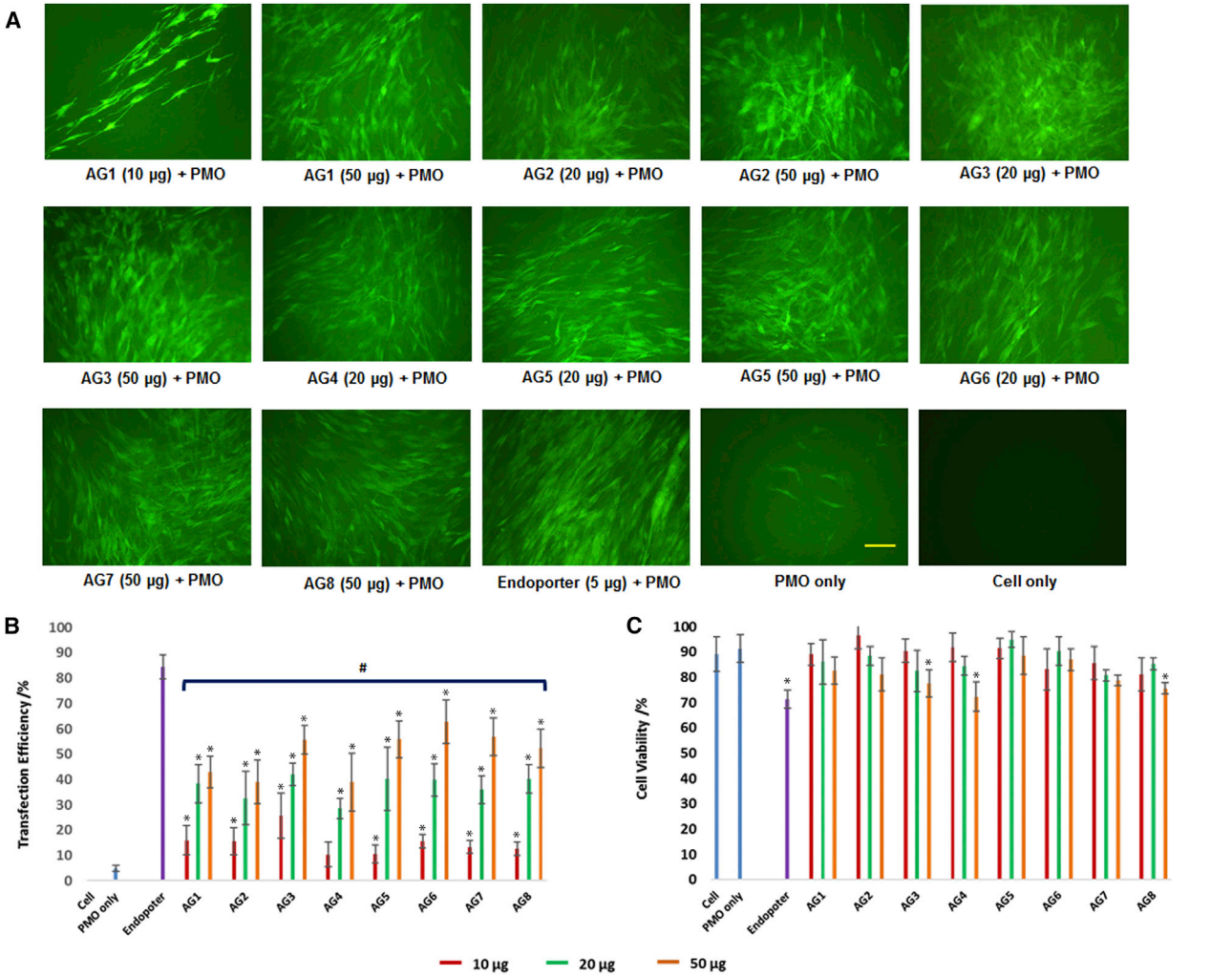

Figure 3. Delivery Efficiency and Toxicity of AG/PMOE50 Complexes in the C2C12E50 Cell Line, Determined by Fluorescence Microscopy and FACS Analysis

(A) Representative fluorescence images of PMO-induced reporter GFP expression with exon 50 skipping in the C2C12E50 cell line. The images were taken after 3-day treatment (original magnification, ×200; scale bar, 200 μm). (B) Transfection efficiency of PMOs formulated with AGs (one-way ANOVA, #$p \leq 0.05$, a significant difference between AG groups; Student's t test, *$p \leq 0.05$ compared with PMO only). (C) Cell viability (one-way ANOVA, no significant difference between AG groups; Student's t test, *$p \leq 0.05$ compared with untreated cells as a control). In this test, 5 μg PMOE50 was formulated with AGs (10, 20, and 50 μg), and Endoporter (5 μg) was formulated as a control in 0.5 mL 10% FBS-DMEM. The results are presented as the mean ± SD in triplicate.

complex particles for a longer circulation time than naked PMO in a biological environment. This may well lead to sustained serum levels and improvement in the uptake of PMO from the vasculature and across the cell membrane, resulting in more effective delivery of PMO into muscles.

Systemic Delivery

DMD affects muscles body-wide, including cardiac muscle. Systemic treatment is therefore indispensable. Based on the results *in vitro* and *in vivo* locally, the four most effective AGs (AG1, AG3, AG5, and AG7) were evaluated further for systemic delivery of PMO by intravenous (i.v.) injection at a dose of 0.5 mg formulated with 1 mg PMOE23 (Figure 6). The control PMOE23 alone induced dystrophin expression in less than 3% of muscle fibers in all skeletal muscles and no detectable dystrophin in cardiac muscle 2 weeks after injection. PMOE23 formulated with AGs produced 10%–25% dystrophin-positive fibers in skeletal muscles, with the highest levels (over 20%) by AG7 in intercostal muscles, quadriceps, and biceps and by AG5 in gastrocnemius muscles. Importantly, immunohistochemistry demonstrated membrane-localized dystrophin in about 2%–4% of cardiac muscle fibers in some areas of the heart treated with a single dose of PMO formulated with AG3 and AG7. This level of dystrophin induction in cardiac muscle, although considerably lower than that in skeletal muscles, could still be beneficial to patients, as suggested previously.[10,17] Overall, AG7-formulated PMO performs the best in both skeletal and cardiac muscles.

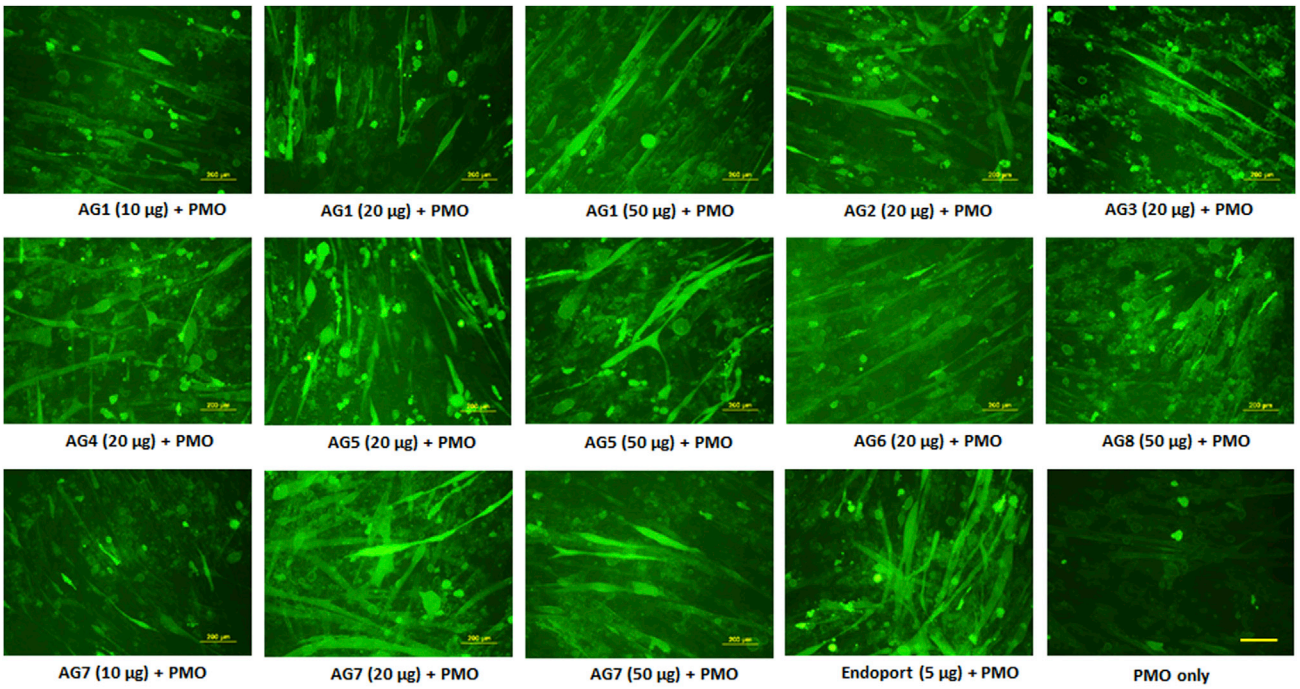

Figure 4. GFP Expression Induced by PMOE23 (5 μg) Formulated with AGs (10, 20, and 50 μg) in C2C12E23 Cells and Endoporter (5 μg) as a Positive Control in 0.5 mL 10% FBS-DMEM after 6-Day Treatment

Original magnification, ×200; scale bar, 200 μm.

No signs of abnormal behavior or change in body weight and overall condition were observed during treatment with any AG/PMO complexes in mice receiving both local and systemic delivery. No pathological changes of the liver, kidneys, and lungs of treated mice were detected by H&E stain with the test dosage as PMO delivery enhancer, although the ototoxicity and nephrotoxicity of some AGs were reported as antibiotics.[53] The results suggest that AGs could potentially be further explored for antisense PMO delivery to increase exon-skipping efficiency, especially for the treatment of muscular dystrophies.

Cellular Uptake and Intracellular Localization

We chose AG7 as a model to study the intracellular localization of the AG/PMO complex in view of its performance with PMO *in vivo*. AG7 was complexed with fluorescein isothiocyanate (FITC)-labeled PMO at a weight ratio of 10:1, and the mixture was used to treat C2C12 cells. The distribution and signal intensity of the fluorescence were then examined and compared with that in cells treated with PMO only (Figure 7). FITC signals in cells treated with PMO alone were hardly detectable. In contrast, signals for PMO formulated with AG7 were considerably stronger and clearly visible within the cytoplasm. Interestingly, the FITC signals in these cells colocalized with the lysosome marker, and limited signals were also observed within the nuclear area of some C2C12 cells treated with AG7-formulated PMO, which indicated the formation of a compacted AG7/PMO complex and release of oligonucleotide from the complex. Therefore, AG showed ability to efficiently deliver oligonucleotide PMO, which might be attributed to AG activity in cell membrane transport.

Interaction between AG and PMO

The affinity between carrier and oligonucleotide is an important parameter for their efficient delivery into cells or tissues. To understand how AGs improve the delivery performance of oligonucleotide PMO, we first examined the interactions between the carrier and PMO at the different weight by UV-visible (UV-vis) spectrum, and AG7 was chosen because of its absorbance at UV to be easily examined; we exemplified the AG7/PMO complex at weight ratios from 5:5 to 50:5 (Figure 8A). All ratios of AG7/PMO complexes showed a very similar absorbance as the PMO without any red or blue shift, except for a hypochromic effect observed at a ratio of 20:5, which indicates high compaction this ratio. The compaction was confirmed by an absorbance analysis, with double peak around 210 nm for AG7/PMO at a ratio of 50:5 because of excess AG7. We further investigated all AGs complexed with PMO at a ratio of 20:5 (Figure 8B). The results showed that all AG/PMO complexes had a very similar absorbance as PMO only, and some of them had a small hypochromic effect compared with PMO alone, which was demonstrated by the very condensed complex formed at this ratio. The results indicate that these AGs, although different in structure, have a similar affinity for PMO because of their nature as amino sugars and similar composition. Second, we further examined an AG/PMO polyplex at a weight ratio of 20:5 in 0.9% saline solution under transmission electron

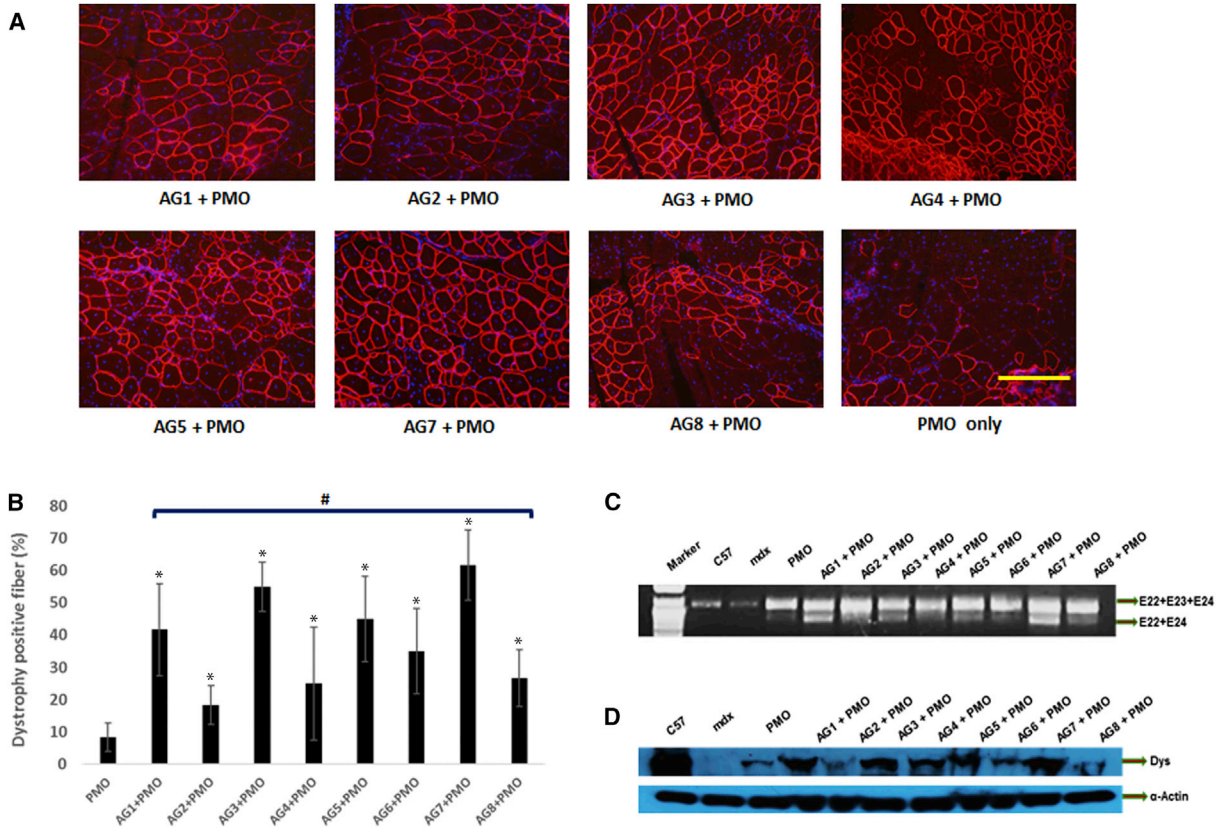

Figure 5. Restoration of Dystrophin in TA Muscles of *mdx* Mice 4–5 Weeks of Age 2 Weeks after i.m. Injection

The samples were from muscles treated with 50 μg AG and 2 μg PMOE23 in 40 μL saline; PMOE23-only (2 μg) treatment was used as a controls. (A) Dystrophin was detected by immunohistochemistry with the rabbit polyclonal antibody P7 against dystrophin. Blue nuclear staining with DAPI (original magnification, ×100; scale bar, 200 μm). (B) The percentage of dystrophin-positive fibers in muscles treated with AG-formulated PMOE23. The numbers of dystrophin-positive fibers were counted in a single cross-section (one-way ANOVA, #$p \leq 0.05$, a significant difference between AG groups; mean ± SD, n = 5, Student's t test, *$p \leq 0.05$ compared with 2 μg PMO). (C) Detection of exon 23 skipping by RT-PCR. Total RNA of 100 ng from each sample was used for amplification of dystrophin mRNA from exon 20 to exon 26. The upper bands (1,093 bp, indicated by E22+E23+E24) correspond to the normal mRNA, and the lower bands (880 bp, indicated by E22+E24) correspond to the mRNA with exon E23 skipped. (D) Western blots demonstrating the expression of dystrophin protein from treated *mdx* mice in comparison with C57BL/6 and untreated *mdx* mice (10 μg of total protein was loaded for PMO, AG-formulated PMO, and control *mdx* samples; 10 μg for the WT C57 control also). Dys, dystrophin detected with the monoclonal antibody Dys 1. α-Actin was used as a loading control.

microscopy (TEM), and AG7/PMO at a ratio of 5:5 and 50:5 was also assessed. As illustrated in Figure 8C, the PMO oligonucleotides alone formed particles with different sizes from less than 10 nm to over 50 nm, which is most likely a result of hydrophobic interaction and hydrogen bonding among PMO molecules. All AG/PMO complexes, however, showed clear, single-sized particles between10–15 nm in diameter at a ratio of 20:5. The particle size of AG7/PMO varies from small to large as the ratio of the two components increases from 5:5 to 50:5. The large particles with a 50:5 ratio are probably a result of aggregation of excessive AG7. An earlier study reported that the binding of AGs to target RNAs is mediated by (1) hydrogen bonding between amino and hydroxyl functional groups of AGs and RNA bases[56] and (2) electrostatic interactions between the negatively charged phosphate backbone of the RNA and the positively charged amino functional groups of the AGs.[57] As for the uncharged oligonucleotide PMO here, the ambiguous binding characteristics of AGs with PMO probably do not originate only from the hydrogen binding-driven mode but also from the inherent conformational adaptability of AGs.[52] Clearly, the mechanisms of interaction between PMO and AGs remain to be further clarified to improve delivery efficiency.

Conclusions

In this study, a few AGs were evaluated for the first time as delivery vectors for antisense PMO-mediated exon skipping. The results show that AGs improve antisense PMO delivery both *in vitro* and in dystrophic *mdx* mice *in vivo*; the delivery efficiency of PMO complexed with AGs improved 15-fold *in vitro* and up to 6-fold *in vivo* compared with that achieved with PMO only. No obvious toxicity was observed with local and systemic delivery at the tested dosages. Thus, AGs could be applied to improve antisense therapy by reducing dosages and lowering the cost, increasing efficacy, which is critically

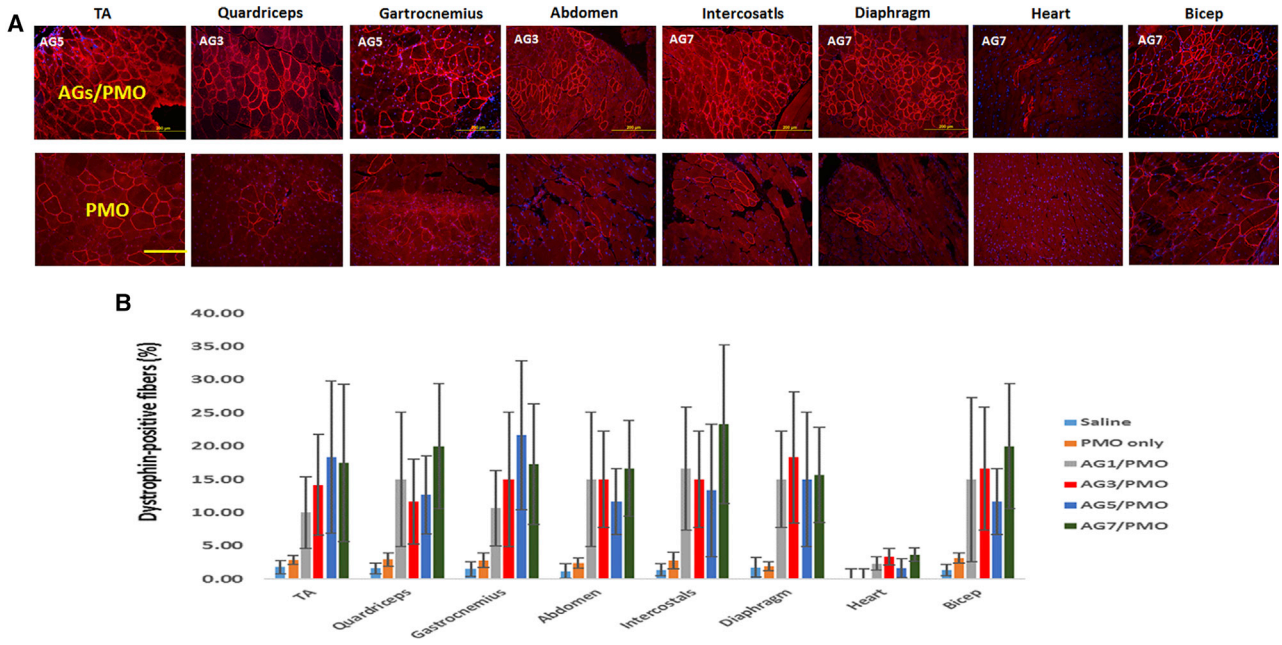

Figure 6. Dystrophin Expression in Different Muscles of *mdx* Mice 4–5 Weeks of Age 2 Weeks after Systemic Administration of PMO with AGs

Each mouse was injected with 1 mg PMOE23 with and without AG (0.5 mg). (A) Immunohistochemistry with the antibody P7 for detection of dystrophin (original magnification, ×100; scale bar, 200 μm). (B) Percentage of dystrophin-positive fibers in different muscle tissues (mean ± SD, n = 5, Student's t test, *p ≤ 0.05 compared with 1 mg PMO).

required for wider application of the antisense therapy. The precise mechanisms by which AGs improve PMO delivery remain to be elucidated. Further optimization and modification of AG structure could potentially eliminate the drug resistance concerns associated with long-term use as enhancers of oligonucleotide delivery.

MATERIALS AND METHODS

Materials

DMEM, penicillin-streptomycin, FBS, L-glutamine, and HEPES (4-(2-hydroxyethyl)-1-piperazineethanesulfonic acid) buffer solution (1 M) were purchased from Thermo Fisher Scientific (Waltham, MA, USA). MTS was bought from BioVision Technologies (Milpitas, CA, USA). The phosphorodiamidate morpholino oligomers PMOE50 (5′-AACTTCCTCTTTAACAGAAAAGCATAC-3′) targeting the human dystrophin gene exon 50, PMOE23 (5′-GGCCAAACCTCGGCTTACCTGAAAT-3′) targeting mouse dystrophin gene exon 23, and Endoporter were purchased from Gene Tools (Philomath, OR, USA). All AGs were purchased from Santa Cruz Biotechnology (Dallas, TX, USA). Other chemicals were purchased from Sigma-Aldrich (St Louis, MO, USA) unless otherwise stated. The investigated AG structures are illustrated in Figure 1.

Cell Lines

C2C12 myoblasts from mouse muscle were purchased from the ATCC (Manassas, VA, USA). The C2C12E50 cell line expresses a human dystrophin exon 50 GFP (hDysE50/GFP)-based reporter. The C2C12E23 cell line expresses a mouse dystrophin exon 23 GFP (mDysE23.GFP)-based reporter. Construction of the mDysE23/hDysE50-GFP-reporter vectors was based on a procedure reported previously.[49]

Cell Viability Assay

Cytotoxicity was evaluated in the C2C12E50 cell line using an MTS-based assay. Cells were seeded in a 96-well tissue culture plate at 1×10^4 cells/well in 200 μL DMEM supplemented with 10% FBS. Cells achieving 70%–80% confluence were exposed to AG at different doses for 24 h, followed by addition of 20 μL of Cell Titer 96Aqueous One Solution (Promega, Madison, WI, USA). After further incubation for 4 h, the absorbance was measured at 570 nm using a Tecan 500 plate reader (Tecan, Morrisville, NC, USA) to obtain the metabolic activity of the cell. Untreated cells were taken as controls with 100% viability and wells without cells as blanks, and the relative cell viability was calculated as follows: $(A_{\text{treated}} - A_{\text{background}}) \times 100/(A_{\text{control}} - A_{\text{background}})$. All viability assays were carried out in triplicate.

In Vitro Transfection

C2C12E50 myoblasts and C2C12E23 differentiated cells expressing the reporter GFP were used in this study. The expression of GFP was controlled by effective skipping of the inserted human dystrophin exon 50 sequence (hDysE50) and mouse dystrophin exon 23 sequence (mDysE23), respectively.[49]

C2C12E50 Cells

The C2C12E50 cell line was maintained in 10% FBS-DMEM in a humidified 10% CO_2 incubator at 37°C. About 5×10^4 cells/well

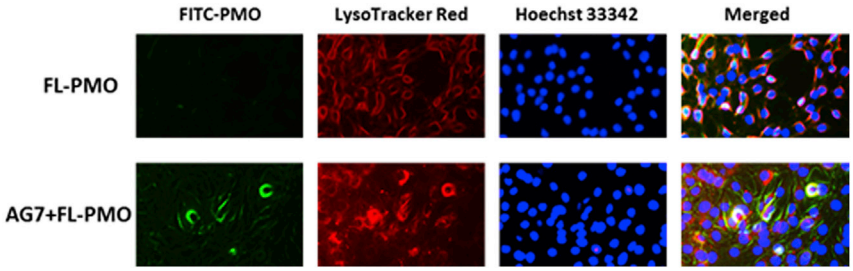

Figure 7. Microscopy Images of PMO-Treated C2C12 Cells with and without AG7 24 h after Delivery
PMO (green), lysosomes (red), and nuclei (blue) stained with FITC-labeled PMO, LysoTracker red, and Hoechst 33342, respectively.

in 500 μL 10% FBS-DMEM were seeded and allowed to grow to a confluence of 70%. Cell culture medium was replaced before addition of AG/PMOE50 (fixed at 5 μg) formulation with varying ratios. Endoporter was used for comparison. Transfection efficiencies, indicated by GFP production, were recorded after 3-day incubation using an Olympus IX71 fluorescent microscope, and digital images were taken with DP Controller and DP Manager software (Olympus, Center Valley, PA, USA). Transfection efficiency was also examined quantitatively using flow cytometry. Cells were washed twice with PBS (1×, pH 7.4), treated with 0.2 mL 0.05% trypsin-EDTA, followed by incubation for 3 min at 37°C. The cells were then treated with cooled growth medium (1 mL), collected by centrifugation, and then resuspended in 0.5 mL of ice-cold PBS (1×, pH 7.4). Samples were run on a FACSCalibur flow cytometer (BD Biosciences, Franklin Lakes, NJ, USA). At least 1×10^4 cells were counted and analyzed with the CellQuest Pro software package (BD Biosciences, Franklin Lakes, NJ, USA).

C2C12E23 Cells

The cell culture and delivery protocols were the same as for C2C12E50 cells. Images were taken and cells were collected after 6-day treatment.

In Vivo Delivery

This study was carried out in strict accordance with the recommendations in the Guide for the Care and Use of Laboratory Animals of the NIH. The protocols were approved by the Institutional Animal Care and Use Committee (IACUC) of Carolinas Medical Center (breeding protocol 10-13-07A, experimental protocol 10-13-08A).

Animals and Injections

Mice were housed with 12-h light-dark cycles in individually ventilated cages and had access to standard chow and water *ad libitum*. Dystrophic *mdx* mice (C57BL/10 as genetic background) aged 4–5 weeks were used for *in vivo* testing (5 mice per group, mixed male and female (m/f), 3 m + 2 f or 2 m + 3 f in the test and control groups) unless stated otherwise. All injections were performed under isoflurane anesthesia, and all efforts were made to minimize suffering.[11–13,49] PMOE23 targeting the boundary sequences of exon and intron 23 of the mouse dystrophin gene (Gene Tools, Philomath, OR) was used. For i.m. injections, 2 μg PMOE23 with or without AG was formulated in 40 μL saline for each TA muscle. For i.v. injection, 1 mg PMO with or without AG (0.5 mg) in 100 μL saline was used. The muscles were examined 2 weeks later, snap-frozen in liquid nitrogen-cooled isopentane, and stored at −80°C.

Immunohistochemistry and Histology

Serial sections of 6 μm were cut from the treated mouse muscles. The sections were stained with a rabbit polyclonal antibody, P7, for the detection of dystrophin protein as described previously.[11,13,14] Polyclonal antibodies were detected by goat anti-rabbit immunoglobulin G (IgG) Alexa 594 (Invitrogen, Carlsbad, CA, USA). For dystrophin-positive fiber counting, dystrophin-positive fibers in one section were counted using an Olympus BX51 fluorescence microscope (Olympus).

Western Blot and RT-PCR for In Vivo Samples

Protein extraction and western blotting were done as described previously.[11,13,14] The collected sections were ground into powder and lysed with 200 μL protein extraction buffer (1% Triton X-100, 50 mM Tris [pH 8.0], 150 mM NaCl, and 0.1% SDS), boiled at 100°C in water for 1 min, and then centrifuged at 18,000 × *g* at 4°C for 15 minutes. The supernatant was quantified for protein concentration with a protein assay kit (Bio-Rad, Hercules, CA, USA). Proteins were loaded onto a 4%–15% Tris-HCl gradient gel. Samples were electrophoresed for 4 h at 120 V at room temperature. Then the gel was blotted onto a nitrocellulose membrane for 4 h at 150 V at 4°C. The membrane was probed with NCL-DYS1 monoclonal antibody against the dystrophin rod domain (1:200 dilutions, Vector Laboratories, Burlingame, CA). The bound primary antibody was detected by horseradish peroxidase (HRP)-conjugated goat anti-mouse IgG (1:3,000 dilutions, Santa Cruz Biotechnology, Dallas, TX, USA) and the enhanced chemiluminescence (ECL) Western blotting analysis system (PerkinElmer, Waltham, MA, USA). The intensity of the bands obtained from treated *mdx* mice muscles was measured with NIH ImageJ software 1.42 (NIH, Bethesda, MD, USA) and compared with that of normal muscles from C57BL/6 mice. α-actin was detected by rabbit anti-actin antibody (Sigma, St. Louis, MO, USA) as a sample loading control.

Total RNA was extracted from the muscle after dissection; 100 ng of RNA template was used for a 25-μL RT-PCR with Fidelitaq RT-MasterMix (USB, Cleveland, OH, USA). The primer sequences for the RT-PCR were Ex20Fo 5′-CAGAATTCTGCCAATTGCT GAG-3′ and Ex26Ro 5′-TTCTTCAGCTTGTGTCATCC-3′ for amplification of mRNA from exons 20 to 26. The cycle conditions for reverse transcription were 43°C for 15 min and 94°C for 2 min.

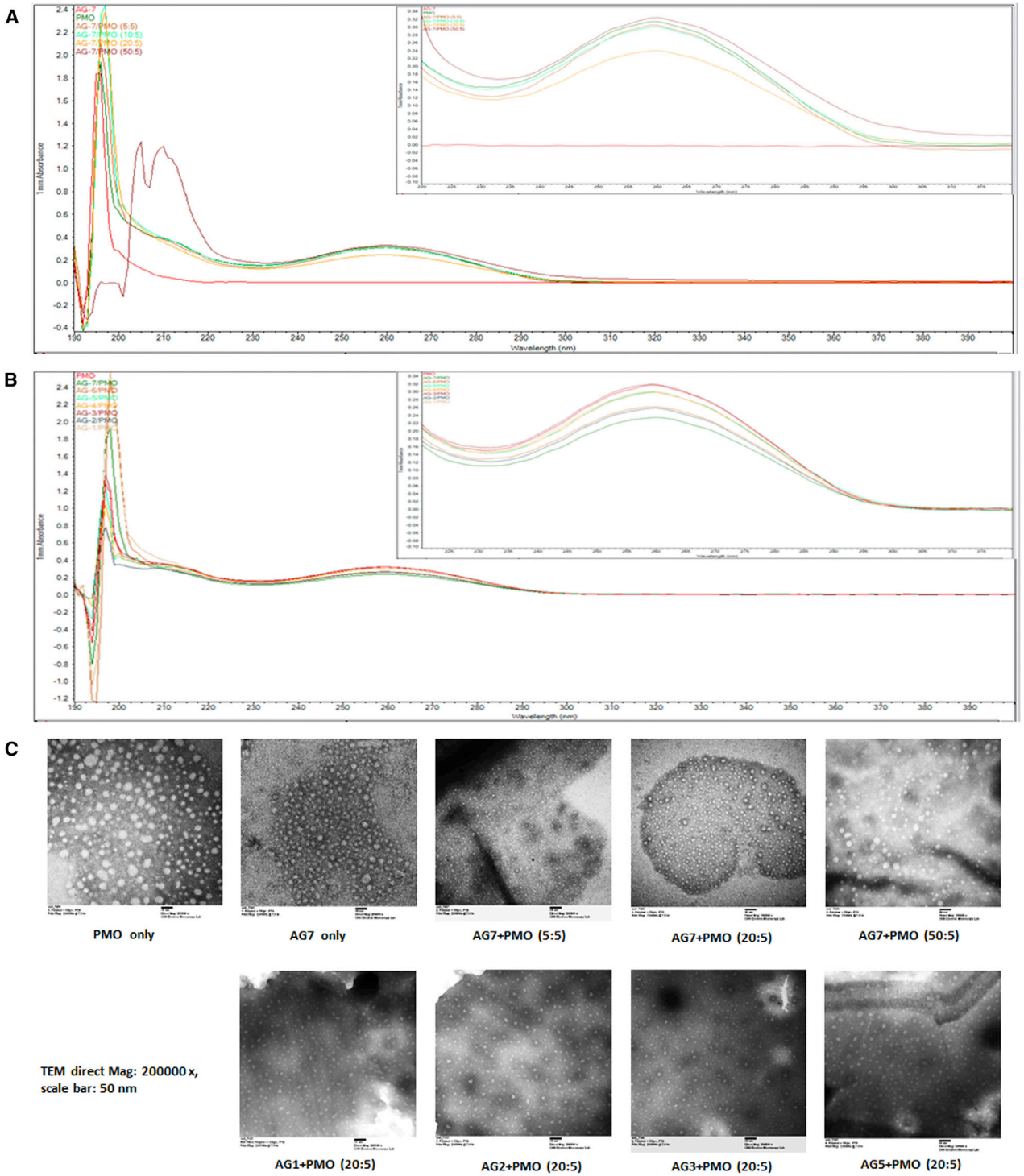

Figure 8. Affinity Study between AGs and PMO

(A) UV-Vis spectra of AG7-formulated PMO at different weight ratios (5:5, 10:5, 20:5, and 50:5) and AG7 and PMO only. (B) UV-Vis spectra of AG-formulated PMO at a weight ratio of 20:5 (1.5-μL sample of deionized [DI] water solution measured at room temperature). (C) Negatively stained transmission electron micrographs (scale bar, 50 nm) of AG-formulated PMO (1 μg) at different weight ratios in 100 μL 0.9% saline.

The reaction was then cycled 30 times at 94°C for 30 s, 65°C for 30 s, and 68°C for 1 min. The products were examined by electrophoresis on a 1.5% agarose gel. The intensity of the bands was measured with NIH ImageJ 1.42, and the percentage of exon skipping was calculated, with the intensity of the two bands representing both exon 23 unskipped and skipped as 100%. The unskipped band including exon 23 was 1093 bp, and the skipped band without exon 23 was 880 bp.

Cellular Uptake and Intracellular Localization

For the cellular uptake and intracellular localization study, C2C12 cells were seeded onto 12-well plates at 5×10^4 cells /well and cultured to 50% confluence before addition of AG-formulated, fluorescence-labeled (FL) PMO complex at the predetermined ratio for testing. 24 h after addition of the samples, cells were washed with warm PBS to remove any residual AG/PMO complex not taken up by cells and incubated with medium containing LysoTracker red DND-99 (Life Technologies, Carlsbad, CA, USA) according to the manufacturer's recommendations to label lysosomes. Cells were also counterstained with Hoechst 33342 (Life Technologies, Carlsbad, CA, USA) to label cell nuclei. Microscopy analysis was performed under an Olympus IX71 fluorescence microscope, and the resulting images of colocalization of AG/PMO to the lysosome were visualized by merged-channel images.

UV-Vis Study

A NanoDrop 2000 spectrophotometer (Thermo Fisher Scientific, Waltham, MA, USA) was used to determine the absorbance of AG and PMO. 1.5 μL of each sample was measured at the desired concentration at room temperature.

TEM

The AG/PMO complex solution containing 1 μg of PMO was prepared at different weight ratios of AG/PMO in 100 μL 0.9% saline and analyzed using TEM (JEM-1400Plus transmission electron microscope, JEOL USA, Inc.) with an AMT-XR80S-B wide-angle side-mount 8-megapixel charge-coupled device (CCD) camera. The samples were prepared using negative staining with 1% phosphotungstic acid. Briefly, one drop of sample solution was placed on a formvar- and carbon-coated carbon grid (Electron Microscopy Sciences, Hatfield, PA, USA) for 1 h and blotted dry, followed by staining for 3 min. Samples were analyzed at 60 kV. Digital images were captured with a digital camera system from 4 pi Analysis (Durham, NC, USA).

Statistical Analysis

All results were expressed as mean ± SD. The data were analyzed using both one-way ANOVA and the Student's t test, with $^*p \leq 0.05$ considered statistically significant.

AUTHOR CONTRIBUTIONS

M.W. conceived and designed the study, drafted the paper, and performed all experiments except for the *in vivo* study. B.W. supervised and performed the *in vivo* experiments with S.N.S. P.L. contributed to cell culture experiments. Q.L. and B.W. reviewed the manuscript.

CONFLICTS OF INTEREST

The authors declare no competing interests.

ACKNOWLEDGMENTS

The authors would like to thank Dr. Fei Guo and Dr. David M. Fourreau for technical assistance with Flow cytometry and analysis and Daisy M. Ridings, Stephanie Williams, and Anthony Dart with the Electron Microscopy Core Laboratory for the negative staining and TEM electron micrographs. The authors also gratefully acknowledge financial support provided by the Carolinas Muscular Dystrophy Research Endowment at the Carolinas HealthCare Foundation and Carolinas Medical Center (Charlotte, NC).

REFERENCES

1. Nowak, K.J., and Davies, K.E. (2004). Duchenne muscular dystrophy and dystrophin: pathogenesis and opportunities for treatment. EMBO Rep. *5*, 872–876.
2. Wagner, K.R., Lechtzin, N., and Judge, D.P. (2007). Current treatment of adult Duchenne muscular dystrophy. Biochim. Biophys. Acta *1772*, 229–237.
3. Gatheridge, M.A., Kwon, J.M., Mendell, J.M., Scheuerbrandt, G., Moat, S.J., Eyskens, F., Rockman-Greenberg, C., Drousiotou, A., and Griggs, R.C. (2016). Identifying Non-Duchenne Muscular Dystrophy-Positive and False Negative Results in Prior Duchenne Muscular Dystrophy Newborn Screening Programs: A Review. JAMA Neurol. *73*, 111–116.
4. Mendell, J.R., Shilling, C., Leslie, N.D., Flanigan, K.M., al-Dahhak, R., Gastier-Foster, J., Kneile, K., Dunn, D.M., Duval, B., Aoyagi, A., et al. (2012). Evidence-based path to newborn screening for Duchenne muscular dystrophy. Ann. Neurol. *71*, 304–313.
5. Long, C., Amoasii, L., Mireault, A.A., McAnally, J.R., Li, H., Sanchez-Ortiz, E., Bhattacharyya, S., Shelton, J.M., Bassel-Duby, R., and Olson, E.N. (2016). Postnatal genome editing partially restores dystrophin expression in a mouse model of muscular dystrophy. Science *351*, 400–403.
6. Goemans, N.M., Tulinius, M., van den Akker, J.T., Burm, B.E., Ekhart, P.F., Heuvelmans, N., Holling, T., Janson, A.A., Platenburg, G.J., Sipkens, J.A., et al. (2011). Systemic administration of PRO051 in Duchenne's muscular dystrophy. N. Engl. J. Med. *364*, 1513–1522.
7. Kinali, M., Arechavala-Gomeza, V., Feng, L., Cirak, S., Hunt, D., Adkin, C., Guglieri, M., Ashton, E., Abbs, S., Nihoyannopoulos, P., et al. (2009). Local restoration of dystrophin expression with the morpholino oligomer AVI-4658 in Duchenne muscular dystrophy: a single-blind, placebo-controlled, dose-escalation, proof-of-concept study. Lancet Neurol. *8*, 918–928.
8. Lu, Q., Mann, C.J., Lou, F., Bou-Gharios, G., Morris, G.E., Xue, S.A., Fletcher, S., Partridge, T.A., and Wilton, S.D. (2003). Functional amounts of dystrophin produced by skipping the mutated exon in the mdx dystrophic mouse. Nat. Med. *9*, 1009–1014.
9. Lu, Q., Rabinowitz, A., Chen, Y.C., Yokota, T., Yin, H., Alter, J., Jadoon, A., Bou-Gharios, G., and Partridge, T. (2005). Systemic delivery of antisense oligoribonucleotide restores dystrophin expression in body-wide skeletal muscles. Proc. Natl. Acad. Sci. USA *102*, 198–203.
10. Mendell, J.R., Rodino-Klapac, L.R., Sahenk, Z., Roush, K., Bird, L., Lowes, L.P., Alfano, L., Gomez, A.M., Lewis, S., Kota, J., et al.; Eteplirsen Study Group (2013). Eteplirsen for the treatment of Duchenne muscular dystrophy. Ann. Neurol. *74*, 637–647.
11. Wu, B., Moulton, H.M., Iversen, P.L., Jiang, J., Li, J., Li, J., Spurney, C.F., Sali, A., Guerron, A.D., Nagaraju, K., et al. (2008). Effective rescue of dystrophin improves cardiac function in dystrophin-deficient mice by a modified morpholino oligomer. Proc. Natl. Acad. Sci. USA *105*, 14814–14819.
12. Wu, B., Li, Y., Morcos, P.A., Doran, T.J., Lu, P., and Lu, Q. (2009). Octa-guanidine morpholino restores dystrophin expression in cardiac and skeletal muscles and ameliorates pathology in dystrophic mdx mice. Mol. Ther. *17*, 864–871.
13. Wu, B., Lu, P., Benrashid, E., Malik, S., Ashar, J., Doran, T.J., and Lu, Q. (2010). Dose-dependent restoration of dystrophin expression in cardiac muscle of dystrophic mice by systemically delivered morpholino. Gene Ther. *17*, 132–140.

14. Wu, B., Lu, P., Cloer, C., Shaban, M., Grewal, S., Milazi, S., Shah, S.N., Moulton, H.M., and Lu, Q. (2012). Long-term rescue of dystrophin expression and improvement in muscle pathology and function in dystrophic mdx mice by peptide-conjugated morpholino. Am. J. Pathol. *181*, 392–400.

15. Yin, H., Moulton, H.M., Seow, Y., Boyd, C., Boutilier, J., Iverson, P., and Wood, M.J. (2008). Cell-penetrating peptide-conjugated antisense oligonucleotides restore systemic muscle and cardiac dystrophin expression and function. Hum. Mol. Genet. *17*, 3909–3918.

16. Evers, M.M., Toonen, L.J.A., and van Roon-Mom, W.M.C. (2015). Antisense oligonucleotides in therapy for neurodegenerative disorders. Adv. Drug Deliv. Rev. *87*, 90–103.

17. Cirak, S., Arechavala-Gomeza, V., Guglieri, M., Feng, L., Torelli, S., Anthony, K., Abbs, S., Garralda, M.E., Bourke, J., Wells, D.J., et al. (2011). Exon skipping and dystrophin restoration in patients with Duchenne muscular dystrophy after systemic phosphorodiamidate morpholino oligomer treatment: an open-label, phase 2, dose-escalation study. Lancet *378*, 595–605.

18. Malerba, A., Sharp, P.S., Graham, I.R., Arechavala-Gomeza, V., Foster, K., Muntoni, F., Wells, D.J., and Dickson, G. (2011). Chronic systemic therapy with low-dose morpholino oligomers ameliorates the pathology and normalizes locomotor behavior in mdx mice. Mol. Ther. *19*, 345–354.

19. Summerton, J., and Weller, D. (1997). Morpholino antisense oligomers: design, preparation, and properties. Antisense Nucleic Acid Drug Dev. *7*, 187–195.

20. Yano, J., and Smyth, G.E. (2012). New antisense strategies: chemical synthesis of RNA oligomers. Adv. Polym. Sci. *249*, 1–48.

21. Wang, M., Wu, B., Lu, P., Cloer, C., Tucker, J.D., and Lu, Q. (2013). Polyethylenimine-modified pluronics (PCMs) improve morpholino oligomer delivery in cell culture and dystrophic mdx mice. Mol. Ther. *21*, 210–216.

22. Wang, M., Wu, B., Tucker, J.D., Lu, P., Cloer, C., and Lu, Q. (2014). Evaluation of Tris [2-(acryloyloxy)ethyl]isocyanurate cross-linked polyethylenimine as antisense morpholino oligomer delivery vehicle in cell culture and dystrophic mdx mice. Hum. Gene Ther. *25*, 419–427.

23. Wang, M., Wu, B., Tucker, J.D., Lu, P., Bollinger, L.E., and Lu, Q. (2015). Tween 85 grafted PEIs enhanced delivery of antisense 2′-O-methyl phosphorothioate oligonucleotides in vitro and in dystrophic mdx mice. J. Mater. Chem. B Mater. Biol. Med. *3*, 5330–5340.

24. Wang, M., Wu, B., Tucker, J.D., Lu, P., and Lu, Q. (2015). Cationic polyelectrolyte-mediated delivery of antisense morpholino oligonucleotides for exon-skipping in vitro and in mdx mice. Int. J. Nanomedicine *10*, 5635–5646.

25. Kendall, G.C., Mokhonova, E.I., Moran, M., Sejbuk, N.E., Wang, D.W., Silva, O., Wang, R.T., Martinez, L., Lu, Q.L., Damoiseaux, R., et al. (2012). Dantrolene enhances antisense-mediated exon skipping in human and mouse models of Duchenne muscular dystrophy. Sci. Transl. Med. *4*, 164ra160.

26. Cao, L., Han, G., Lin, C., Gu, B., Gao, X., Moulton, H.M., Seow, Y., and Yin, H. (2016). Fructose Promotes Uptake and Activity of Oligonucleotides With Different Chemistries in a Context-dependent Manner in mdx Mice. Mol. Ther. Nucleic Acids *5*, e329.

27. Han, G., Gu, B., Cao, L., Gao, X., Wang, Q., Seow, Y., Zhang, N., Wood, M.J., and Yin, H. (2016). Hexose enhances oligonucleotide delivery and exon skipping in dystrophin-deficient mdx mice. Nat. Commun. *7*, 10981.

28. Wang, M., Wu, B., Shah, S.N., Lu, P., and Lu, Q. (2018). Saponins as Natural Adjuvant for Antisense Morpholino Oligonucleotides Delivery in Vitro and in mdx Mice. Mol. Ther. Nucleic Acids *11*, 192–202.

29. Sommer, M.O.A., Dantas, G., and Church, G.M. (2009). Functional characterization of the antibiotic resistance reservoir in the human microflora. Science *325*, 1128–1131.

30. Mingeot-Leclercq, M.P., Glupczynski, Y., and Tulkens, P.M. (1999). Aminoglycosides: activity and resistance. Antimicrob. Agents Chemother. *43*, 727–737.

31. Tamma, P.D., Cosgrove, S.E., and Maragakis, L.L. (2012). Combination therapy for treatment of infections with gram-negative bacteria. Clin. Microbiol. Rev. *25*, 450–470.

32. Drew, R.H. (2018). Aminoglycosides. UpToDate, https://www.uptodate.com/contents/aminoglycosides.

33. Fuchs, A., Bielicki, J., Mathur, S., Sharland, M., and Van Den Anker, J.N. (2018). Reviewing the WHO guidelines for antibiotic use for sepsis in neonates and children. Paediatr. Int. Child Health *38*, S3–S15.

34. Loebenberg, D., Counels, M., and Waitz, J.A. (1975). Antibiotic G418, a new micromomospora-produced aminglycoside with activity against protozoa and helminths: antiparasitic activity. Antimicrob. Agents Chemother. *7*, 811–815.

35. Saap, L., Fahim, S., Arsenault, E., Pratt, M., Pierscianowski, T., Falanga, V., and Pedvis-Leftick, A. (2004). Contact sensitivity in patients with leg ulcerations: a North American study. Arch. Dermatol. *140*, 1241–1246.

36. Ryu, D.H., and Rando, R.R. (2001). Aminoglycoside binding to human and bacterial A-Site rRNA decoding region constructs. Bioorg. Med. Chem. *9*, 2601–2608.

37. Dunant, P., Walter, M.C., Karpati, G., and Lochmüller, H. (2003). Gentamicin fails to increase dystrophin expression in dystrophin-deficient muscle. Muscle Nerve *27*, 624–627.

38. Malik, V., Rodino-Klapac, L.R., Viollet, L., and Mendell, J.R. (2010). Aminoglycoside-induced mutation suppression (stop codon readthrough) as a therapeutic strategy for Duchenne muscular dystrophy. Ther. Adv. Neurol. Disorder. *3*, 379–389.

39. Kimura, S., Ito, K., Miyagi, T., Hiranuma, T., Yoshioka, K., Ozasa, S., Matsukura, M., Ikezawa, M., Matsuo, M., Takeshima, Y., and Miike, T. (2005). A novel approach to identify Duchenne muscular dystrophy patients for aminoglycoside antibiotics therapy. Brain Dev. *27*, 400–405.

40. Chittapragada, M., Roberts, S., and Ham, Y.W. (2009). Aminoglycosides: molecular insights on the recognition of RNA and aminoglycoside mimics. Perspect. Medicin. Chem. *3*, 21–37.

41. Fourmy, D., Recht, M.I., Blanchard, S.C., and Puglisi, J.D. (1996). Structure of the A site of Escherichia coli 16S ribosomal RNA complexed with an aminoglycoside antibiotic. Science *274*, 1367–1371.

42. Recht, M.I., Fourmy, D., Blanchard, S.C., Dahlquist, K.D., and Puglisi, J.D. (1996). RNA sequence determinants for aminoglycoside binding to an A-site rRNA model oligonucleotide. J. Mol. Biol. *262*, 421–436.

43. Sannes-Lowery, K.A., Mei, H.Y., and Loo, J.A. (1999). Studying aminoglycoside antibiotic binding to HIV-1 TAR RNA by electrospray ionization mass spectrometry. Int. J. Mass Spectrom. *193*, 115–122.

44. Wang, Y., Hamasaki, K., and Rando, R.R. (1997). Specificity of aminoglycoside binding to RNA constructs derived from the 16S rRNA decoding region and the HIV-RRE activator region. Biochemistry *36*, 768–779.

45. von Ahsen, U., Davies, J., and Schroeder, R. (1992). Non-competitive inhibition of group I intron RNA self-splicing by aminoglycoside antibiotics. J. Mol. Biol. *226*, 935–941.

46. Mikkelsen, N.E., Brännvall, M., Virtanen, A., and Kirsebom, L.A. (1999). Inhibition of RNase P RNA cleavage by aminoglycosides. Proc. Natl. Acad. Sci. USA *96*, 6155–6160.

47. Corvaisier, S., Bordeau, V., and Felden, B. (2003). Inhibition of transfer messenger RNA aminoacylation and trans-translation by aminoglycoside antibiotics. J. Biol. Chem. *278*, 14788–14797.

48. Hainrichson, M., Nudelman, I., and Baasov, T. (2008). Designer aminoglycosides: the race to develop improved antibiotics and compounds for the treatment of human genetic diseases. Org. Biomol. Chem. *6*, 227–239.

49. Hu, Y., Wu, B., Zillmer, A., Lu, P., Benrashid, E., Wang, M., Doran, T., Shaban, M., Wu, X., and Lu, Q. (2010). Guanine analogues enhance antisense oligonucleotide-induced exon skipping in dystrophin gene in vitro and in vivo. Mol. Ther. *18*, 812–818.

50. Sazani, P., Kang, S.H., Maier, M.A., Wei, C., Dillman, J., Summerton, J., Manoharan, M., and Kole, R. (2001). Nuclear antisense effects of neutral, anionic and cationic oligonucleotide analogs. Nucleic Acids Res. *29*, 3965–3974.

51. Luedtke, N.W., Carmichael, P., and Tor, Y. (2003). Cellular uptake of aminoglycosides, guanidinoglycosides, and poly-arginine. J. Am. Chem. Soc. *125*, 12374–12375.

52. Blount, K.F., Zhao, F., Hermann, T., and Tor, Y. (2005). Conformational constraint as a means for understanding RNA-aminoglycoside specificity. J. Am. Chem. Soc. *127*, 9818–9829.

53. Barton-Davis, E.R., Cordier, L., Shoturma, D.I., Leland, S.E., and Sweeney, H.L. (1999). Aminoglycoside antibiotics restore dystrophin function to skeletal muscles of mdx mice. J. Clin. Invest. *104*, 375–381.

54. Vicens, Q., and Westhof, E. (2002). Crystal structure of a complex between the aminoglycoside tobramycin and an oligonucleotide containing the ribosomal decoding a site. Chem. Biol. *9*, 747–755.

55. François, B., Russell, R.J., Murray, J.B., Aboul-ela, F., Masquida, B., Vicens, Q., and Westhof, E. (2005). Crystal structures of complexes between aminoglycosides and decoding A site oligonucleotides: role of the number of rings and positive charges in the specific binding leading to miscoding. Nucleic Acids Res. *33*, 5677–5690.

56. Jiang, L., and Patel, D.J. (1998). Solution structure of the tobramycin-RNA aptamer complex. Nat. Struct. Biol. *5*, 769–774.

57. Wang, H., and Tor, Y. (1997). Electrostatic Interactions in RNA Aminoglycosides Binding. J. Am. Chem. Soc. *119*, 8734–8735.